Electronic Supplementary Material (ESI) for Journal of Materials Chemistry A.

Supporting Information

3D Hollow MXene (Ti_3C_2)/ Reduced Graphene Oxide Hybrid Nanospheres for High-Performance Li-Ion Storage

Miao Guo[a], *Shulin Zhong*[a], *Tian Xu*[a], *Yuqin Huang*[a], *Tengfei Zhang*[b]*, *Guanglin Xia*[a], *Xuebin Yu*[a]*

[a] Department of Materials Science, Fudan University, Shanghai 200433, China

[b] College of Materials Science and Technology, Nanjing University of Aeronautics and Astronautics, Nanjing 210016, China

* Corresponding authors

*E-mail: zhangtengfei@nuaa.edu.cn (T. Zhang), *E-mail: yuxuebin@fudan.edu.cn (X. B. Yu)

Materials and methods

Preparation of Ti_3C_2 MXene： 0.5 g Ti_3AlC_2 powder (11 technology, co., L TD) was added into 10 mL 9 M HCl solution containing 0.5 g LiF and reacted at 35 ℃ for 24 h. Subsequently, the mixture was centrifugally washed repeatedly with deionized water until the pH of the solution was >6. After centrifugation, the precipitate was ultrasonized in the ice bath for 2 h under the protection of argon. The ultrasonic suspension was centrifuged at 3500 RPM for 1 h, and the dark green upper suspension was freeze-dried to obtain the MXene material.

Preparation of PS template: 9 g of styrene solution (99%, Sinopharm Chemical Reagent Co., Ltd) was mixed with 180 mL of water in a three-necked flask. N_2 was added and stirred for 1 h. The temperature was then raised to 60 ℃, and 180 mg of 2, 2-azodiisobutylamidine dihydrochloride (97%, Sinopharm Chemical Reagent Co., Ltd) was dissolved in 15 g of water and the solution was added to a three-neck flask. PS nanospheres were obtained after 6 h reaction at 70 ℃. The whole reaction is under the protection of argon. The product was centrifugally washed repeatedly for 3 times, and the precipitate was collected and stored in an aqueous solution.

Preparation of 3D hollow MXene-rGO Nanospheres: The MXene dispersion was mixed with PS dispersion for 30 min to obtain PS@MX dispersion. The GO dispersion was added into the mixture and continued stirring for 30 min. The PS@MX@GO dispersion was obtained after 20 min of ultrasonic dispersion and 30 min of magnetic stirring. Then the powder PS@MX@GO composite material was obtained by freeze-drying. Finally, the powder material was placed in a tubular furnace with inert gas, calcined at 500 °C for 2 h at a heating rate of 5 °C/min. The PS template was removed by high temperature heating and GO was reduced to obtain the final product s-MX@rGO. According to the different proportion of MXene in the composite material (**Table S1**, Supporting Information), s-MX@rGO composites are recorded as s-MX@rGO-1, 2 and 3. The corresponding PS@MX@GO composites are recorded as PS@MX@GO-1, 2 and 3, respectively.

Material Characterization: The morphology and structure of materials and electrodes were characterized by SEM (Scanning Electron Microscope, JEOL 7500FA), TEM (Transmission Electron Microscope, JEM-211F). Energy-filtered TEM (JEOL 2011 F, Tokyo, Japan) was used to investigate the microstructure and for elemental mapping. The phase structures of the powdery composite were analyzed by XRD (D8 Advance, Bruker AXS) with Cu Kα radiation and Jobin Yvon Horiba Raman spectrometer model HR800, with a 10 mW helium/neon laser at 632.8 nm excitation in the range of 100 to 2500 cm^{-1}. The compositions of the composites were determined by thermogravimetry analysis (TGA, Netzsch STA 449 F3) between RT and 600 °C at a heating rate of 10°C min^{-1} under a nitrogen atmosphere. The nitrogen adsorption/desorption isotherms were obtained at -195.85°C under the relative pressure (P/P_0) range from 0 to 1 with an Autosorb-1specific surface area analyzer from MICROMERITICS ASAP2460. The Zeta potential was obtained by adjusting the PH of PS, MXene and rGO aqueous dispersions to 7 by Malvern Zetasizer Nano ZS90.

Electrochemical Measurement: All the cells were assembled with standard

CR2032 coin-type half cells to evaluate their electrochemical performance at room temperature. Lithium foils, Celgard 2400 Polypropylene membranes, and 1m $LiPF_6$ in ethylene carbonate/ diethyl carbonate/ methyl hexyl carbonate (1:1:1, v/v/v) with 5% fluoroethylene carbonate were used as counter electrode, separator, and electrolyte, respectively. The working electrodes were composed of active materials, super p, and polyvinylidene fluoride (PVDF) binder in a weight ratio of 7:2:1 with N-methyl-2-pyrrolidinone (NMP) as dispersant. The half-cells were assembled in an Ar-filled glove box with H_2O and O_2contents below 0.1 ppm. Galvanostatic charge/discharge tests were carried out on a Land battery tester between 0.01 and 3.0 V versus Li/Li+. The CV curves at a scan rate of 0.1 mV s^{-1}、0.2 mV s^{-1}、0.5 mV s^{-1}、1 mV s^{-1}、2 mV s^{-1}、5 mV s^{-1}、10 mV s^{-1} in the range of 0.01V-3 V. The EIS by applying an ac amplitude of 5 mV over the frequency range of 100 kHz to 0.01 Hz were carried out on a CHI 660E electrochemical workstation.

Computational Methods: All Density functional theory (DFT) calculations were performed with Vienna ab initio Simulation Package (VASP). The generalized gradient approximation (GGA) with a Perdew-Burke-Ernzerh (PBE) of exchange correlation functional and projector-augmented wave (PAW) method were used. During the optimization process, the structures were relaxed until the forces and total energy on all atoms were converged to less than 0.05 eV $Å^{-1}$ and 1×10^{-5} eV. A cut-off energy of 400 eV and Gamma centered 3×3×1 k-points mesh were set for all calculation. Zero damping DFT-D3 dispersion correction method of Grimme was used to simulate Van der Waals (VdW) interactions in the system. To simulate the interface between MXene and graphene, we construct a model with one MXene slab (Ti_3C_2, according to the raw materials and characterization results) and one graphene layer, and build a vacuum layer in c axis which is thick enough (15 Å) to prevent potential interaction between layers in different cells. To minimize the lattice mismatch between MXene and graphene, a hexagonal supercell of a = b = 9.90 Å, c = 19.74 Å with 50 C atoms, 27 Ti atoms have to be constructed. And adsorption positions for Li on MXene slab have 3 possible locations: i) on top of Ti atom; ii) above the bridge position between 2 Ti atoms; iii) above the center of Ti triangle. Adsorption energy, which is defined as: $E_{ads} = E_{tot} - E_{s\text{-}MX@G} - E_{Li}$, of all 3 locations were compared, and results showed that the center positions were energy favorable. Hence, another supercell with one Li atom located at center position is built to analyze electronic difference after Li adsorption.

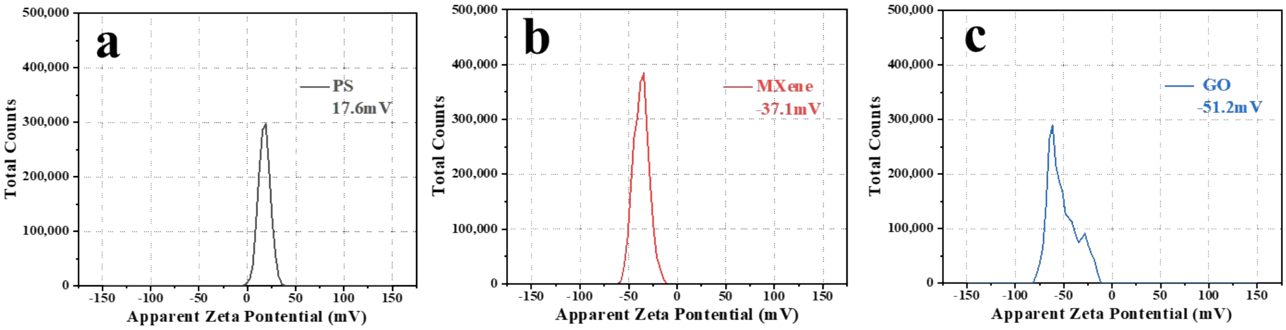

Figure S1. The Zeta potentials of the PS, film MXene, and GO aqueous dispersion

Table S1. Concentrations and scales of the precursors PS, MXene and GO.

Sample	PS (35 mg/mL)	MXene (5 mg/mL)	GO (5 mg/mL)
s-MX	3	9	0
s-rGO	3	0	9
s-MX@rGO-1	2.7 mL	4 mL	4 mL
s-MX@rGO-2	3 mL	3 mL	6 mL
s-MX@rGO-3	3.3 mL	2 mL	8 mL

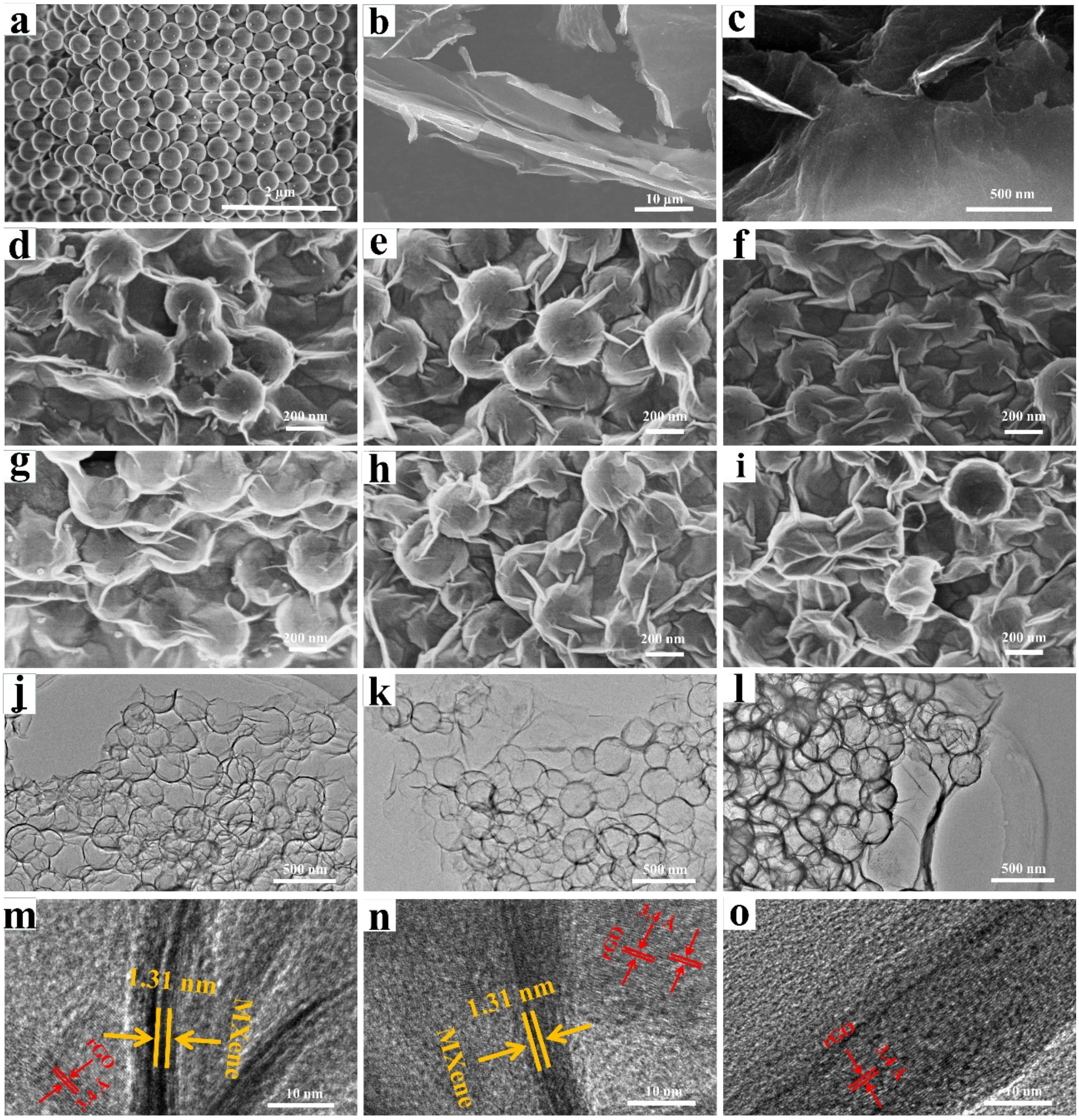

Figure S2. **a)** SEM image of PS, **b)** SEM image of MX, **c)** SEM image of GO, **d)** SEM image of PS@MX@GO-2, **e)** SEM image of PS@MX@GO-3, **f)** SEM image of PS@GO, **g)** SEM image of s-MX@GO-2, **h)** SEM image of s-MX@GO-3, **i)** SEM image of s-GO, **j)** TEM image of s-MX@GO-2, **k)** TEM image of s-MX@GO-3, **l)**TEM image of s-GO, **m)** high-resolution TEM image of s-MX@GO-2, **n)** high-resolution TEM image of s-MX@GO-3, **o)** high-resolution TEM image of s-GO.

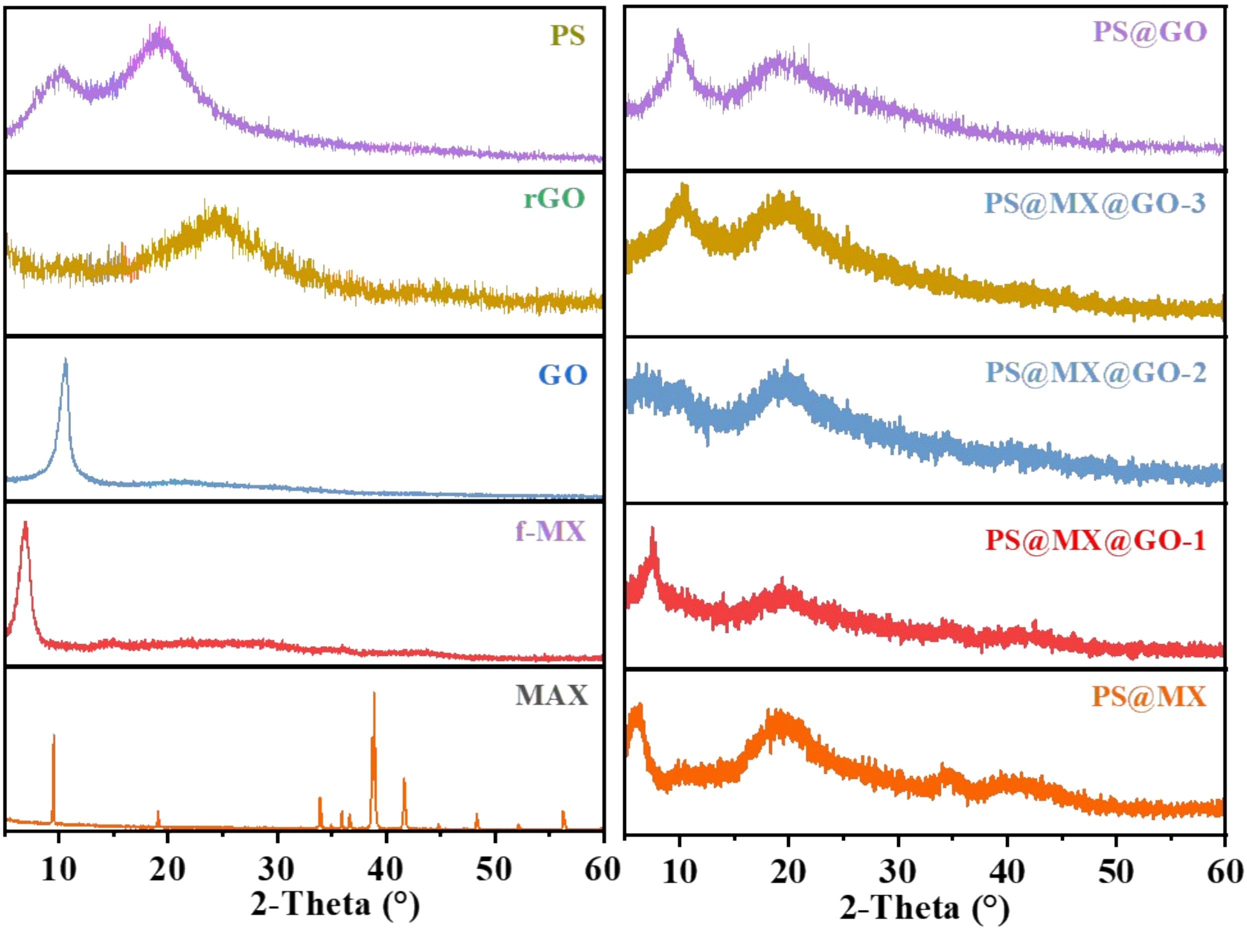

Figure S3. XRD patterns of as-prepared samples.

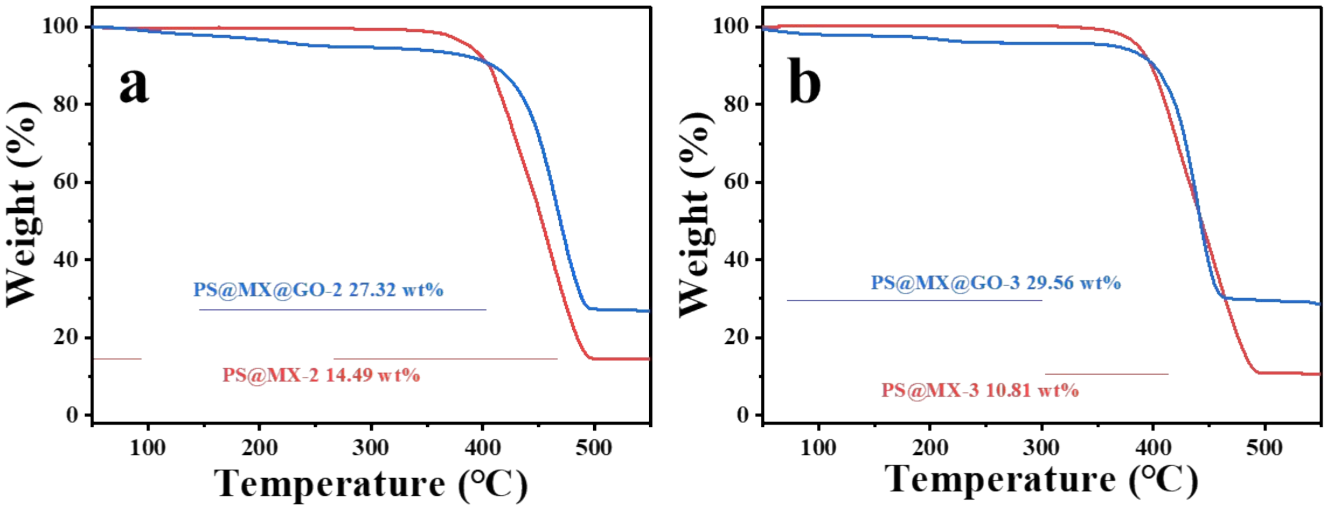

Figure S4. a) TGA curves of s-MX@rGO-2. **b)** TGA curves of s-MX@rGO-3.

As shown in **Figure 3c**, the weight of the s-MX@rGO-1 above 500 °C in air remained unchanged. The weight loss can mainly be attributed to the vaporization of PS and the reduction of rGO. It is found that the PS@MX@GO nanocomposite mass decreased by 69.0 wt% while the mass of PS@MX decreased by 77.3 wt% after heat treatment. Due to the volatilization of PS, only MXene remains after calcination of PS@MX material, so the ratio of MXene in PS@MX is 22.7 wt%. In the precursor of PS@MX@GO-1, the ratio of MXene to GO is 1:1 (Table S1). Assuming that the combined weight of PS and MX in PS@MX@GO is 100 mg, where PS is 77.3 mg and MXene is 22.7 mg, and the amount of GO and MXene is the same, the total mass of the PS@MX@GO system is 122.7 mg. After heat treatment, the composite became MX@rGO with a weight of 122.7 mg × 31 wt% = 38.0 mg due to the PS evaporation and the GO reduced to the rGO. The proportion of MXene in the composite is calculated according to the following formula:

$$\omega = \frac{m_{MXene}}{m_{composite}}$$

Therefore, the ratio of MXene in MX@rGO is 22.7 mg/38.0 mg = 59.7 wt%. The same method calculates the proportion of MXene in s-MX@rGO-2 and s-MX@rGO-3 samples, which are 41.1 wt% and 25.5 wt%, respectively.

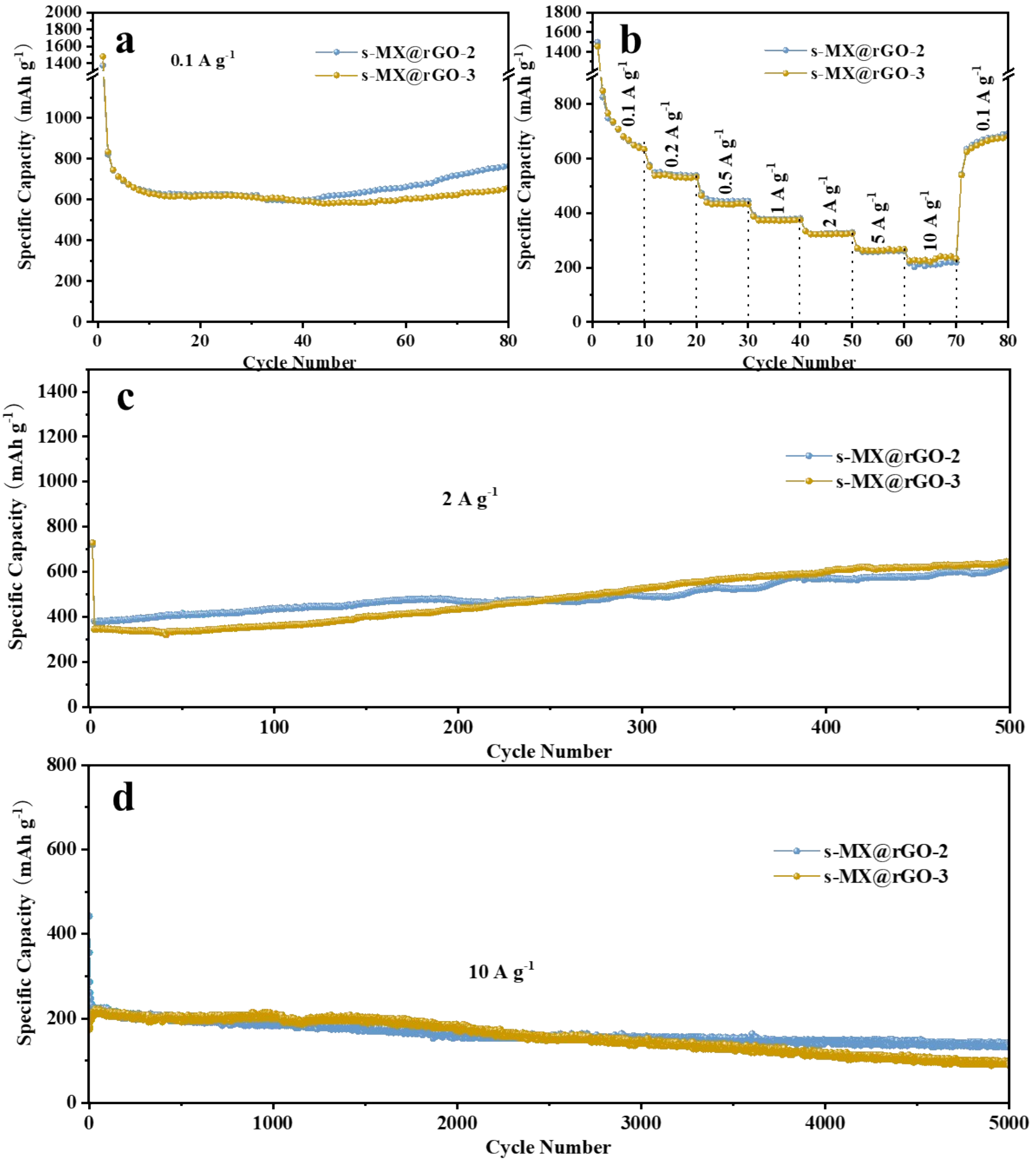

Figure S5. a) cyclic performance of s-MX@rGO-2, 3 electrodes at 100 mA g^{-1}; **b)** rate capability of s-MX@rGO-2, 3 at various current densities (0.1 A g^{-1} ~10 A g^{-1}); **c)** cyclic performance of s-MX@rGO-2, 3 electrodes at 2 A g^{-1}; **d**) long-term cyclic property of s-MX@rGO-2, 3 electrodes at 10 A g^{-1} for 5000 cycles.

Table S2. Comparison of s-MX@rGO-1 electrode with other reported MXene-based anodes (1C = 320 mAh g^{-1}).

Anode materials	Long cyclic performance	Rate performance		references
	Capacity(mAh g^{-1})/Cycles/ Current density	Rate	Capacity (mAh g^{-1})	
Ti_3C_2/CNTs	428/300/0.5C	0.1C	713.2	1
		0.2C	543.1	
		0.5C	407.7	
		1C	320.6	
		2C	218.2	
p-$Ti_3C_2T_x$/CNTs	500/100/0.5C	0.1C	1250	2
		10C	330	
Ti_3C_2/CNF	97/2900/100C	1C	320	3
		3.5C	180	
		8.5C	145	
		30C	106	
Ti_3C_2	410/100/10C 110/100/36C			4
Ti_3C_2 foam	220/3500/3.13C 455/300/0.16C	3.13C	215.6	5
		6.25C	187.4	
		31.25C	133.3	
		46.88C	112.5	
		56.28C	101	
Ti_2C	80/120/3C 70/200/10C	0.04C	225	6
		1C	110	
		3C	80	
		10C	70	
Ti_3C_2	88/100/3C 69/100/10C	1C	123.6	7
		3C	88	
		10C	69	
$Ti_3C_2T_x$	424.8/50/0.33C	0.33C	1080	8
		2.7C	864	
$Ti_3C_2NT_x$	343/1000/0.16C 300/1000/1.56C	0.16C	215	9
		1.56C	174	
		3.13C	142	
		6.25C	107	
3D porous MXene/ rGO hybrid aerogels	897/30/0.1C 596/500/1C	0.1C	1270	10
		0.2C	1102	
		0.5C	974	
		1C	977	

3D porous MXene/rGO hybrid film	212/1000/3.1C	0.31C	≈275	11
		0.63C	≈245	
		1.56C	≈200	
		2.50C	≈165	
		3.13C	≈150	
		6.25C	≈125	
		12.50C	≈100	
rGO/Ti$_2$CTx	700/200/0.31C	0.16C	853	12
		0.31C	700	
		0.78C	558	
		1.56C	482	
		3.13C	401	
		6.25C	325	
rGO/Ti$_3$C$_2$Tx	305/100/0.31C	0.16C	480	
		1.56C	230	
		6.25C	160	
MXene-TiO$_2$/rGO	162.8/200/1C 130.6/1000/5C	0.25	302.8	13
		0.5	229.1	
		1C	200.4	
		2.5C	185.2	
		5C	170.7	
		10C	148.4	
		25C	128.3	
		50C	114.4	
3D hollow MXene/rGO sphere	**773/80/0.31C** **672.1/500/6.25C** **241.5/5000/31.25C**	**0.1C**	**659.6**	**This work**
		0.2C	**520.7**	
		0.5C	**428.4**	
		1C	**366.2**	
		2C	**318.3**	
		5C	**259.7**	
		10C	**212.5**	

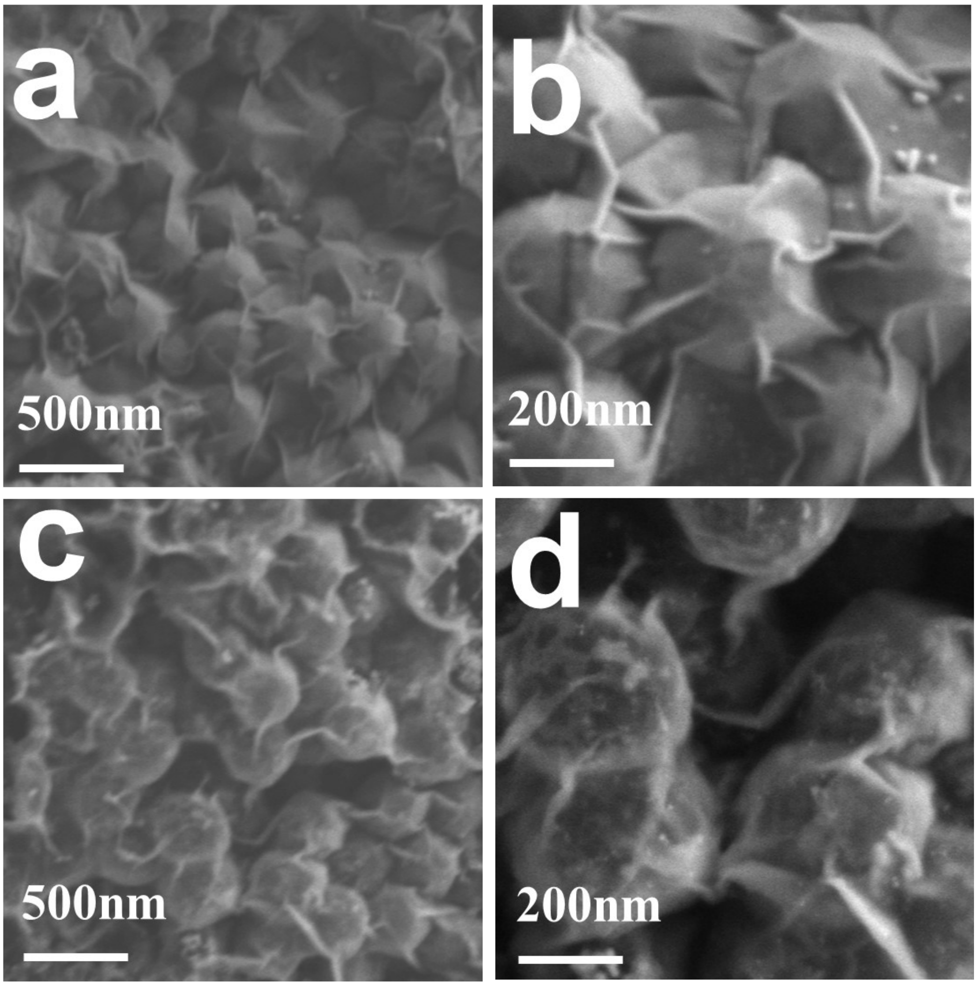

Figure S6. SEM images of the s-MX@rGO-1 electrode at 2 A g^{-1} after 100 cycles at 20000x **(a)** and 50000x **(b)** magnification; SEM images of the s-MX@rGO-1 electrode at 2 A g^{-1} after 500 cycles at 20000x **(c)** and 50000x **(d)** magnification.

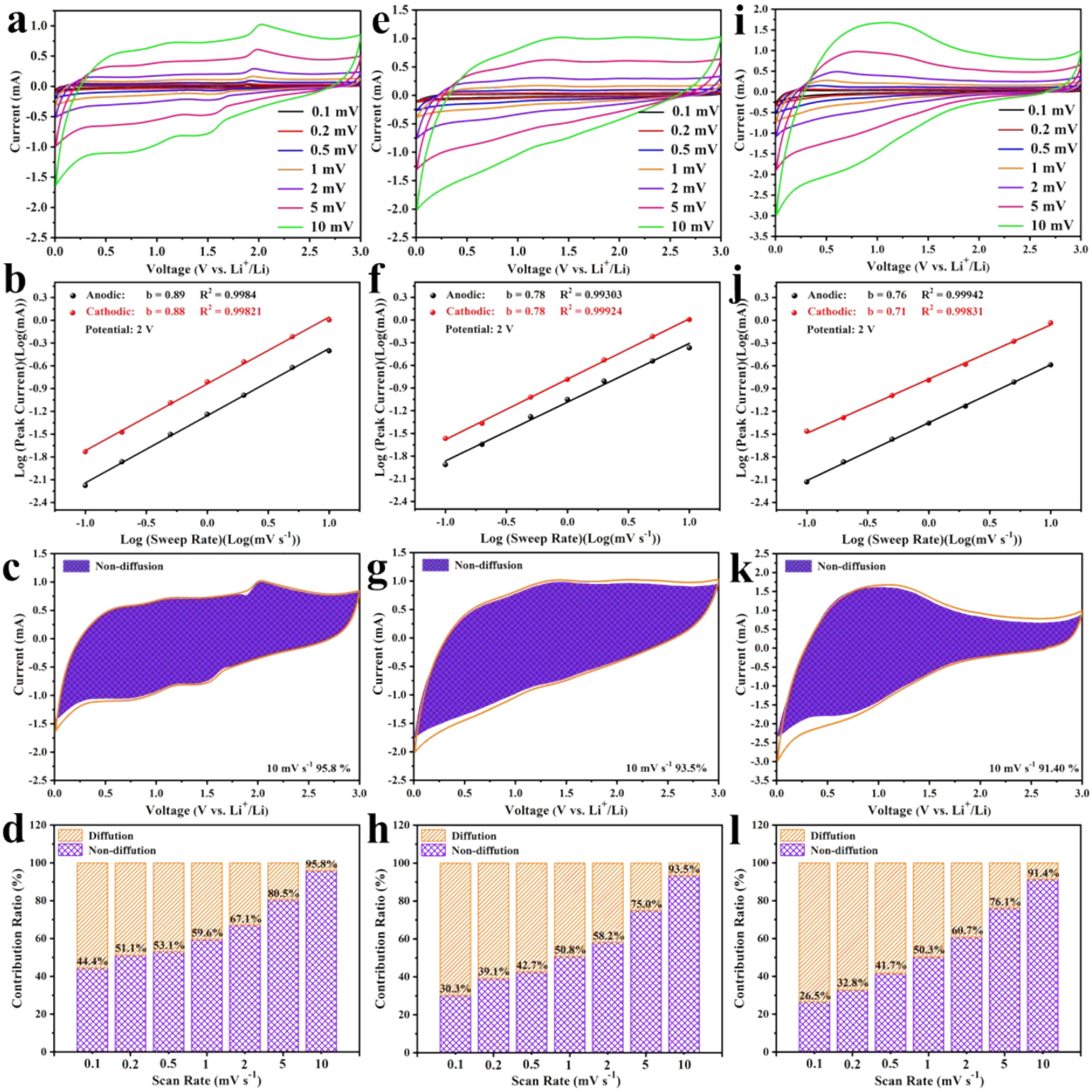

Figure S7. CV curves of the f-Mx, s-Mx, and s-rGO (a, e and i) electrodes at various scan rates, Log i vs log v graph for the cathodic peak of the f-Mx, s-Mx, and s-rGO (b, f and j) electrodes. At a sweep rate of 10 mV s^{-1}. the capacity plots (c, g and k) contributed by non-ionic diffusion. Figure of the proportions of non-ionic diffusion and ionic diffusion at different sweep speeds (d, h and l).

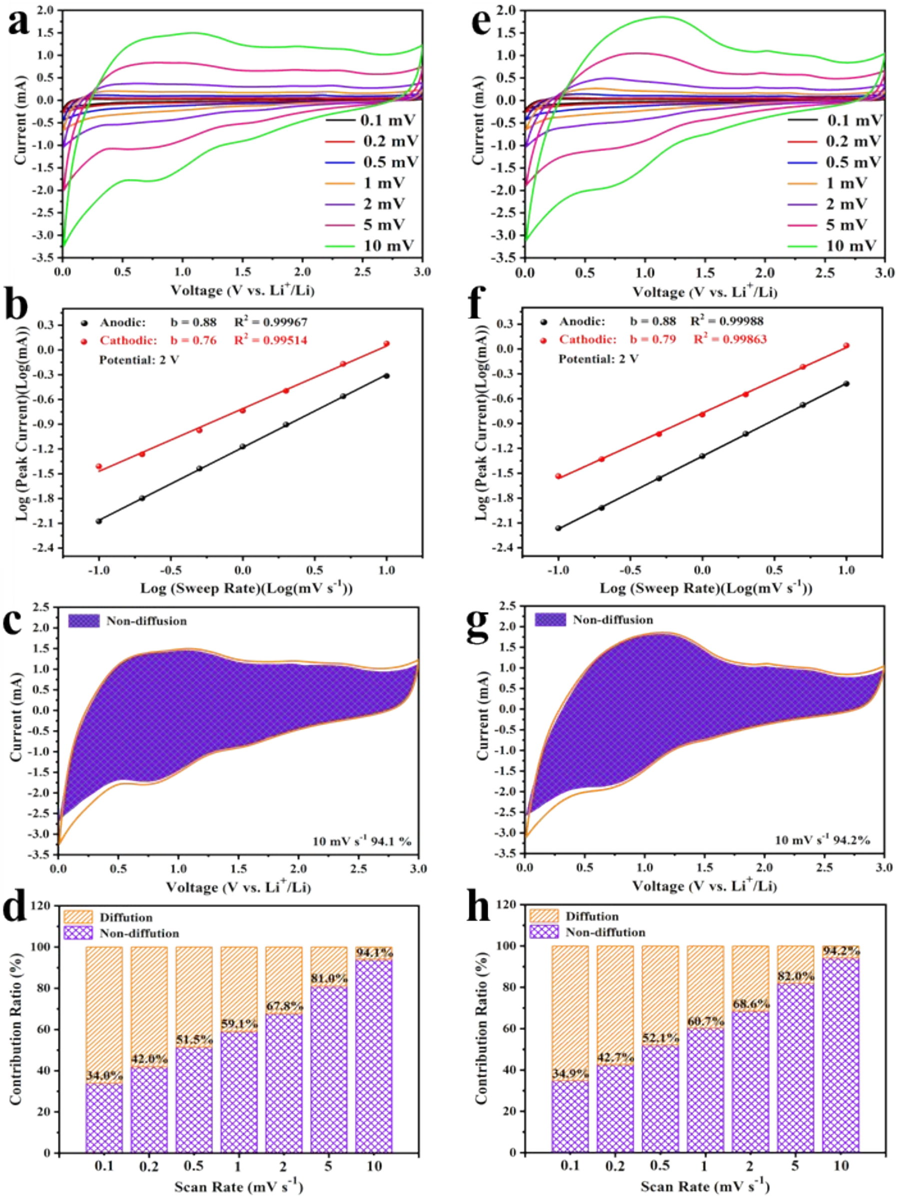

Figure S8. CV curves of the s-MX@rGO-2、3 (**a** and **e**) electrodes at various scan rates. Log i vs log v graph for the cathodic peak of the s-MX@rGO-2、3 (**b** and **f**) electrodes. At a sweep rate of 10 mV s^{-1}, the capacity plots (**c** and **g**) contributed by non-ionic diffusion. Figure of the proportions of non-ionic diffusion and ionic diffusion at different sweep speeds (**d** and **h**).

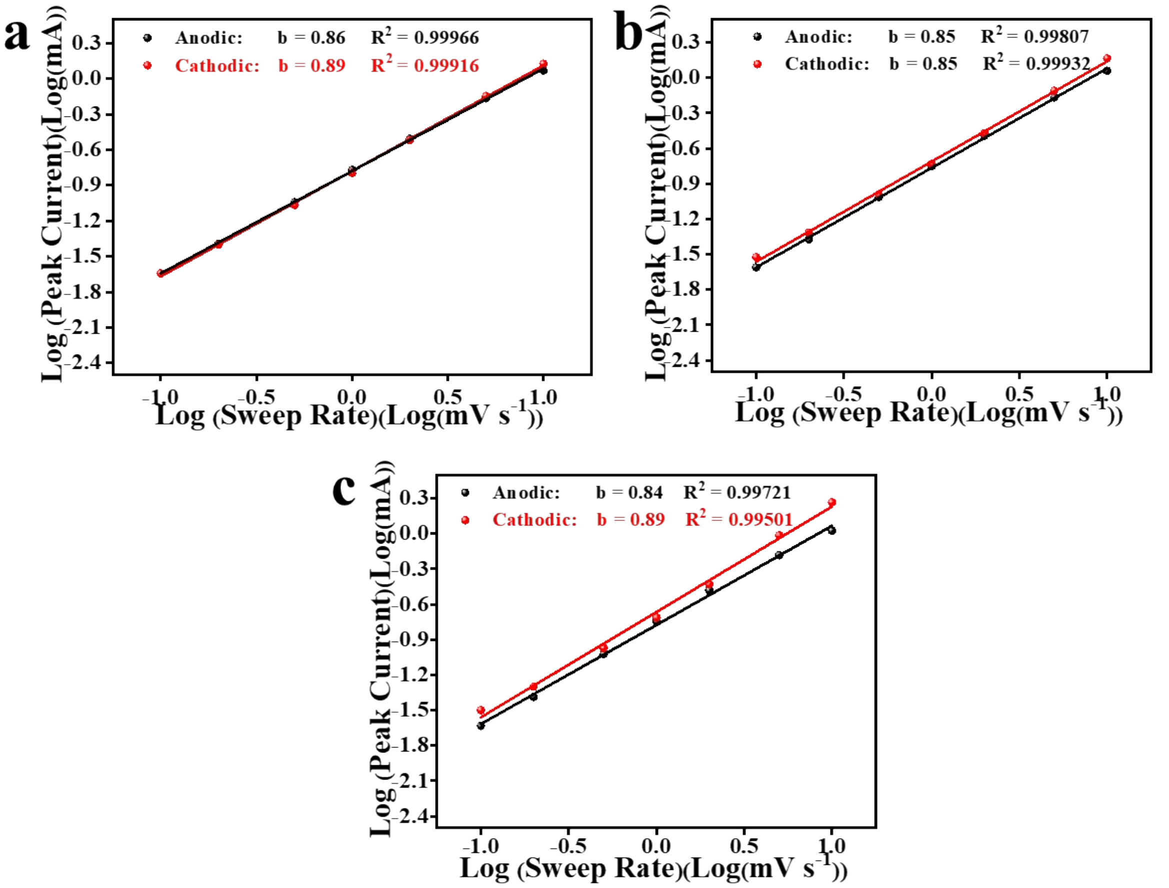

Figure S9. The relationship between the peak current and scan rates from 0.1 to 10 mV s^{-1} for the s-MX@rGO-1 (a), 2 (b), and 3 (c) electrodes at 1.2 V.

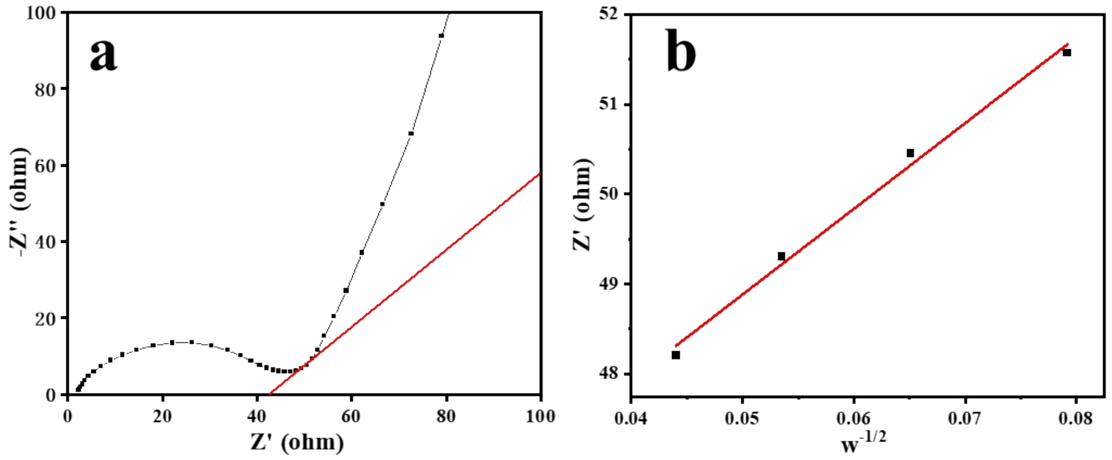

Figure S10. (a) Nyquist plots of s-MX@rGO-1 electrodes. (b) Plot of imaginary resistance as function of inverse square root of angular speed for s-MX@rGO-1 electrodes.

The Li$^+$ diffusion coefficient of the material is calculated according to the following formula:

$$D = \frac{R^2T^2}{2n^2A^2F^4C^2\sigma^2}$$

R - The gas constant, 8.314 J k^{-1}mol^{-1}.

T - Kelvin temperature, in case of room temperature test, t = 298K.

A -The electrode surface area.

n - The number of electrons transferred during the reaction.

F - Faraday constant 96500 c mol^{-1}.

σ-Is a straight-line fit Z '~ $\omega^{-1/2}$ slope.

C-The phase concentration of lithium ion.

The specific values substituted into the above formula to calculate the Li$^+$ diffusion coefficient of s-MX@rGO-1 at room temperature is 1.33×10^{-13} cm^2 s^{-1}. The Li$^+$ diffusion coefficients of s-MX and s-rGO are calculated in the same way, and the values are 3.88×10^{-14} cm^2 s^{-1} and 3.8×10^{-12} cm^2 s^{-1}, respectively.

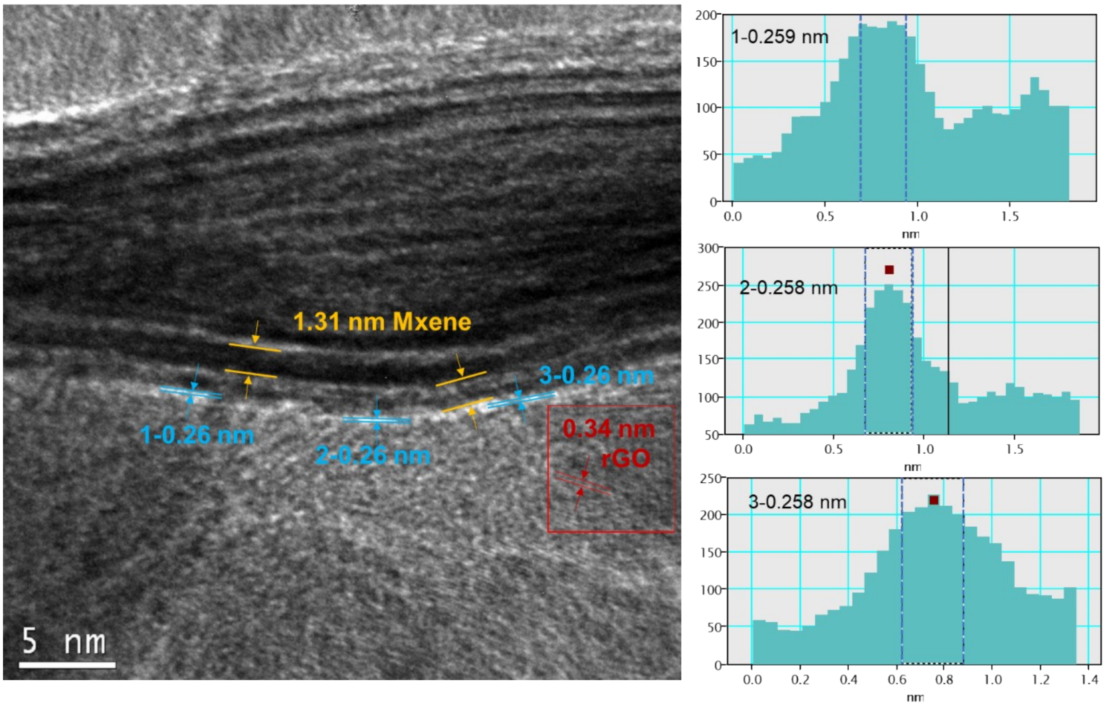

Figure S11. Calculation of layer spacing between MXene and rGO

Supplementary References:

1 Y. Liu, W. Wang, Y. Ying, Y. Wang and X. Peng, *Dalton Trans.*, 2015, **44**, 7123-7126.

2 C. E. Ren, M.-Q. Zhao, T. Makaryan, J. Halim, M. Boota, S. Kota, B. Anasori, M. W. Barsoum and Y. Gogotsi, *Chemelectrochem.*, 2016, **3**, 689-693.

3 Z. Y. Lin, D. F. Sun, Q. Huang, J. Yang, M. W. Barsoum and X. B. Yan, *J. Mater. Chem. A*, 2015, **3**, 14096-14100.

4 O. Mashtalir, M. Naguib, V. N. Mochalin, Y. Dall'Agnese, M. Heon, M. W. Barsoum and Y. Gogotsi, *Nat. Commun.*, 2013, **4**, 1716.

5 Q. Zhao, Q. Zhu, J. Miao, P. Zhang, P. Wan, L. He and B. Xu, *Small*, 2019, **15**, e1904293.

6 J. Come, M. Naguib, P. Rozier, M. W. Barsoum, Y. Gogotsi, P. L. Taberna, M. Morcrette and P. Simon, *J. Electrochem. Soc.*, 2012, **159**, A1368-A1373.

7 D. Sun, M. Wang, Z. Li, G. Fan, L.-Z. Fan and A. Zhou, *Electrochem. Commun.*, 2014, **47**, 80-83.

8 S. J. Kim, M. Naguib, M. Q. Zhao, C. F. Zhang, H. T. Jung, M. W. Barsoum and Y. Gogotsi, *Electrochim. Acta.*, 2015, **163**, 246-251.

9 F. Du, H. Tang, L. M. Pan, T. Zhang, H. M. Lu, J. Xiong, J. Yang and C. Zhang, *Electrochim. Acta.*, 2017, **235**, 690-699.

10 J. Song, X. Guo, J. Zhang, Y. Chen, C. Zhang, L. Luo, F. Wang and G. Wang, *J. Mater. Chem. A*, 2019, **7**, 6507-6513.

11 Z. Ma, X. Zhou, W. Deng, D. Lei and Z. Liu, *ACS Appl. Mater. Interfaces*, 2018, **10**, 3634-3643.

12 S. Xu, Y. Dall'Agnese, J. Li, Y. Gogotsi and W. Han, *Chem.*, 2018, **24**, 18556-18563.

13 Y. Z. Fang, R. Hu, B. Y. Liu, Y. Y. Zhang, K. Zhu, J. Yan, K. Ye, K. Cheng, G. L. Wang and D. X. Cao, *J. Mater. Chem. A*, 2019, **7**, 5363-5372.